Padé-Z_2 estimator of determinants

C. Thron, S. J. Dong, K. F. Liu, and H. P. Ying*

Department of Physics and Astronomy, University of Kentucky, Lexington, Kentucky 40506
(Received 11 July 1997; published 30 December 1997)

We introduce the Padé-Z_2 (PZ) stochastic estimator for calculating determinants and determinant ratios. The estimator is applied to the calculation of fermion determinants from the two ends of the hybrid Monte Carlo trajectories with pseudofermions. Our results on the $8^3 \times 12$ lattice with Wilson action show that the statistical errors from the stochastic estimator can be reduced by more than an order of magnitude by employing an unbiased variational subtraction scheme which utilizes the off-diagonal matrices from the hopping expansion. Having been able to reduce the error of the determinant ratios to about 20% with a relatively small number of noise vectors, this may become a feasible algorithm for simulating dynamical fermions in full QCD. We also discuss the application to the density of states in Hamiltonian systems. [S0556-2821(98)05803-2]

I. INTRODUCTION

At present, lattice gauge Monte Carlo calculation is still the only viable and practical means of solving QCD and computing hadron masses and matrix elements non-perturbatively. As such, there is a perpetual need of sharpening the tools to tackle the numerically intensive aspects of the computation, especially those pertaining to dynamical fermions.

The Euclidean functional integration formulation of the quantum field theory of gauge bosons and fermions has the generic partition function

$$Z = \int [dU][d\bar{\psi}][d\psi] e^{-S_G - \bar{\psi} \mathbf{M} \psi}, \qquad (1)$$

where U is the gauge link variable and S_G the gauge part of the action. Given that the fermion part of the action is quadratic in the Grassmann numbers $\bar{\psi}$ and ψ, they can be formally integrated out to give a fermion determinant, i.e.

$$Z = \int [dU] \det \mathbf{M}[U] e^{-S_G}. \qquad (2)$$

Since numerically the computation of the fermion determinant is much more demanding a task than the updating of gauge links U, it is often approximated by a constant. This is known as the *quenched approximation* which has previously been interpreted as tantamount to neglecting the internal quark loops. Recently, Sexton and Weingarten [1] have advanced the view that it actually corresponds to the inclusion of the leading terms in the loop expansion which are commensurate with the size of loops in the gauge action. This leads to a shift in β or the bare coupling constant. Although a number of low-energy quantities, such as hadron masses [2], weak matrix elements [3,4], and hadron structure [5,6], are reproduced reasonably well (within 6%–15% in many cases) in the quenched approximation, we know that the chi-

ral log behaviors of these quantities [7,8], the η' mass, and the phase transition [9] depend crucially on the full inclusion of dynamical fermions. Thus, solving full QCD with dynamical quarks remains a desirable and challenging ultimate goal.

In view of the perceived difficulty of calculating determinants accurately, all the existing working algorithms have avoided calculating them directly. Instead, pseudofermions [10] and local bosons [11] are introduced to bosonize the determinantal effects. For example, the current state of the art algorithm—the hybrid Monte Carlo (HMC) algorithm [12]—transforms the partition function in Eq. (2) to the following one for 2 degenerate flavors:

$$Z = \int [dU][d\phi][d\phi^\star] e^{-S_G - \phi^\star (\mathbf{M}^\dagger \mathbf{M})^{-1} \phi}, \qquad (3)$$

where ϕ is a pseudofermion variable which can be generated using a Gaussian heat bath. This gives rise to the pseudofermion force which acts over the course of molecular dynamics trajectories to update the gauge field and the fermion matrix $\mathbf{M}$ which in turn enables the updating of the ϕ field.

On the other hand, it may be desirable to admit the determinantal effects directly without resorting to the superfluous degrees of freedom from pseudofermions. This can be done in principle with the partition function in Eq. (2) rewritten as

$$Z = \int [dU] e^{-S_G + \mathrm{Tr} \log \mathbf{M}}, \qquad (4)$$

and Tr log $\mathbf{M}$ which reflects the dynamical fermions is taken as an additional part of the gauge action. It is shown in [13] that a HMC-like algorithm based on the partition function in Eq. (4) is valid provided that Tr log $\mathbf{M}$ can be estimated without bias. However, the task at first sight appears daunting. First of all, one needs an efficient algorithm to calculate Tr log $\mathbf{M}$. This is apparently much more intensive numerically than calculating $(M^\dagger M)^{-1}\phi$ in the pseudofermion approach. In addition, the demands on the accuracy of Tr log $\mathbf{M}$ are very stringent. Since the relative error of det $\mathbf{M}$ is the absolute error in Tr log $\mathbf{M}$, a 20% error in det $\mathbf{M}$ for example would require calculating Tr log $\mathbf{M}$ (which is of the

*On leave from: Zhejiang Institute of Modern Physics, Zhejiang University, China.

order N) to within 0.2. Luckily, the Monte Carlo updating involves only determinant ratios, and not the determinants themselves. One would expect that an accuracy of ~ 0.2 should be somewhat easier to achieve for the difference $\mathrm{Tr}\log \mathbf{M}_1 - \mathrm{Tr}\log \mathbf{M}_2$ than for each term separately.

We shall present in this paper an efficient stochastic algorithm to estimate $\mathrm{Tr}\log\mathbf{M}$ which has the potential of achieving the kind of accuracy (~ 0.2) in $\mathrm{Tr}\log$ difference with relatively small (~ 500) number of noise vectors. This new algorithm invokes the Padé approximation for the log $\mathbf{M}$ and uses complex Z_2 noise to estimate the trace, as introduced in Sec. II. We have tested it by calculating the determinants and determinant ratios of fermion matrices from both ends of randomly chosen molecular dynamics trajectories generated by the hybrid Monte Carlo algorithm with pseudofermions. We also applied the method to Wilson fermions on an $8^3 \times 12$ lattice, and studied its dependence on the rank of the Padé expansion and the number of noise vectors. In Sec. III we introduce an unbiased variational subtraction scheme which is based on the subtraction of traceless terms in the hopping parameter expansion. We find that this can reduce the statistical error by an order of magnitude, leading to an error in the range of 0.2–0.3 with 400–600 noise vectors. These results are presented in Sec. IV. We should mention that there exist other stochastic estimators for determinants. Reference [1] uses the Chebyshev polynominal to expand $\log \mathbf{M}^\dagger\mathbf{M}$ and Gaussian noise to estimate the trace. Reference [14] uses Z_2 noise and the Riemann-Stieltjes integral to estimate the $\mathrm{Tr}\log\mathbf{M}$. The subtraction scheme we introduce here is applicable to both of these approaches. A discussion of application to density of states in Hermitian Hamiltonian systems is presented in Sec. V. Section VI gives the conclusions and outlook.

II. BASIC PADÉ-Z_2 METHOD

A. Padé approximation

The starting point for the current algorithm is the Padé approximation of the logarithm function [[15]]. The Padé approximant to $\log(z)$ of order $[K,K]$ at z_0 is a rational function $N(z)/D(z)$ where $\deg N(z)=\deg D(z)=K$, whose value and first $2K$ derivatives agree with $\log z$ at the specified point z_0. When the Padé approximant $N(z)/D(z)$ is expressed in partial fractions, we obtain

$$\log z \approx b_0 + \sum_{k=1}^{K} \left(\frac{b_k}{z+c_k} \right), \qquad (5)$$

whence it follows

$$\log \det \mathbf{M} = \mathrm{Tr}\log\mathbf{M} \approx b_0 \mathrm{Tr}\mathbf{I} + \sum_{k=1}^{K} b_k \mathrm{Tr}(\mathbf{M}+c_k\mathbf{I})^{-1}. \qquad (6)$$

For the purpose of Monte Carlo updating, only the ratio of determinants is needed. In this case, the log of the determinant ratio $\det\mathbf{M}_1/\det\mathbf{M}_2$ is approximated as

$$\log\{\det\mathbf{M}_1/\det\mathbf{M}_2\} = \mathrm{Tr}[\log\mathbf{M}_1 - \log\mathbf{M}_2]$$
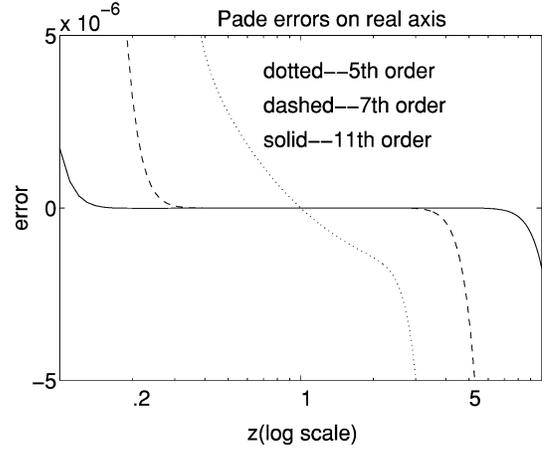
FIG. 1. $\epsilon(z)$ for the Padé approximation of $\log z$ on the positive real axis for different orders of the Padé expansion at $z_0 = 1.0$.

$$\approx \sum_{k} b_k [\mathrm{Tr}(\mathbf{M}_1+c_k\mathbf{I})^{-1}$$
$$- \mathrm{Tr}(\mathbf{M}_2+c_k\mathbf{I})^{-1}], \qquad (7)$$

where $\mathbf{M}_1$ and $\mathbf{M}_2$ are matrices at the beginning and end of a HMC trajectory for example.

This approximation is accurate as long as the eigenvalues of the matrices $\mathbf{M}_1$ and $\mathbf{M}_2$ all lie in the region in the complex plane where the Padé approximation is accurate. If we define $\epsilon(z)$ to be the difference between the right- and left-hand sides of Eq. (5), then the error in the approximation in Eq. (6) is

$$\Delta_{\mathrm{Tr}\log\mathbf{M}} = \sum_{n} \epsilon(\lambda_n), \qquad (8)$$

where $\{\lambda_n\}$ are the eigenvalues of $\mathbf{M}$.

The accuracy of the Padé approximation is graphically illustrated in Figs. 1–6. In Fig. 1, we plot $\epsilon(z)$ for different orders of the Padé approximation on the positive real axis. We see that $\epsilon(z)$ for the 5th order Padé approximation reaches quickly to the order of 10^{-6} around the expansion point $z_0=1$, whereas that of the 7th order does not reach
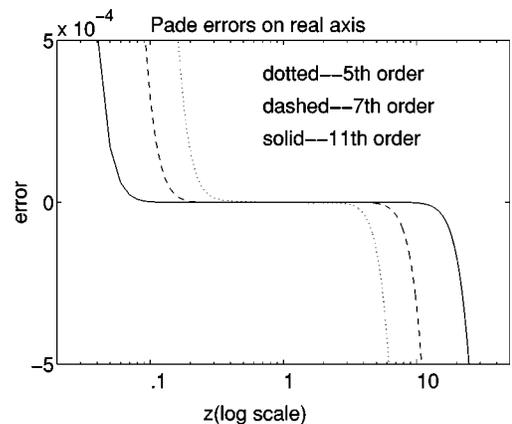
FIG. 2. Same as Fig. 1, on a larger domain.
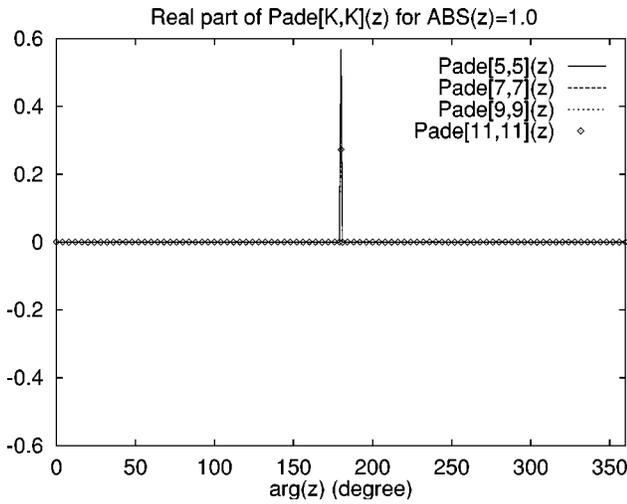
FIG. 3. Real parts of various orders of the Padé approximation to $\log z$ on $|z|=1$ as a function of $\arg(z)$. The Padé expansion point is $z_0=1$.

10^{-6} until z is smaller than 0.3 and greater than 3. For the 11th order, the domain for which $\epsilon(z)<10^{-6}$ is extended to between 0.1 and 10.

Figure 2 is the same plot on a larger domain of z. It shows that $|\epsilon(z)|$ increases with increasing distance to the expansion point. The figure clearly depicts the inversion antisymmetry $\epsilon(1/z)=-\epsilon(z)$, which is due to the corresponding antisymmetry of the logarithm. Hence, if the expansion point is suitably chosen near the ''center'' of the eigenvalue distribution, we shall get error cancellation. The coefficients of the Padé approximation b_k and c_k in Eq. (5) for 5th, 7th, 9th, and 11th orders used to produce Figs. 1 and 2 are tabulated in Table I.

In Figs. 1 and 2, the Padé expansion point is chosen as $z_0=1$. The error functions $\epsilon_{z_0}(z)$ for other expansion points are identical, modulo a change of scale. This is due to the fact that $\log z=\log(z/z_0)+\log(z_0)$, and hence the Padé approximation $P_{z_0}(z)$ for $\log z$ around z_0 is equal to

$$P_{z_0}(z)=P_1(z/z_0)+\log(z_0). \qquad (9)$$

FIG. 5. Same as Fig. 3, for $|z|=10$.

It follows that

$$\epsilon_{z_0}(z)=P_1(z/z_0)-\log(z/z_0)=\epsilon(z/z_0). \qquad (10)$$

We see from these figures that as long as one has some notion about the domain of the eigenvalues of the matrix $\mathbf{M}$ and the desirable level of accuracy one needs for Tr $\log \mathbf{M}$, one can decide on an appropriate order of the Padé approximation and the expansion point z_0.

The Padé approximation of the logarithm is not limited to the real axis. It applies equally well to the complex plane, except near the branch cut. Padé approximation of the logarithm about a positive real z_0 corresponds to a branch cut along the negative real axis, and the poles of the Padé functions all lie on the negative real axis. Using coefficients from Table I which are obtained from expansion about $z_0=1$, we plot the Padé approximated $\log z$ along the unit circle as a function of $\arg(z)$. The real part as shown in Fig. 3 reveals the pole at $z=-1$ for all the Padé functions with different orders. Figure 4 shows the imaginary part. The imaginary part of the log function has a discontinuity from π to $-\pi$ across the negative real axis, while the Padé approximations have discrete poles. Thus, the Padé approximation fails near

FIG. 4. Imaginary parts corresponding to the real parts shown in Fig. 3.
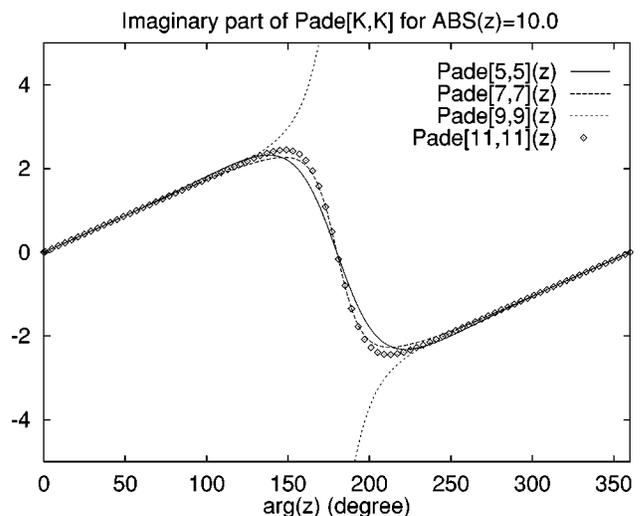
FIG. 6. Same as Fig. 4, for $|z|=10$.

TABLE I. The coefficients b_k and c_k of Padé expansions $P[K,K]$ for $\log z$ at $z_0 = 1.0$.

k	b_k	c_k	b_k	c_k
	$P[5,5]$		$P[7,7]$	
	($b_0 = 4.566666667$)		($b_0 = 5.185714286$)	
1	0.130408172495391	0.0492189449629343	0.06816753269	0.02611045152
2	0.404437841802115	0.299993435237384	0.1844456100	0.1484146919
3	1.13777777850000	1.00000000000000	0.3863893344	0.4226317870
4	4.49394268525114	3.33340630084376	0.8359183641	1.0000000000
5	53.8334305460671	20.3173813294693	2.163220583	2.3661258591
6			8.373644726	6.737877409
7			99.98821380	38.29883980
	$P[9,9]$		$P[11,11]$	
	($b_0 = 5.65793650793651$)		($b_0 = 6.03975468975469$)	
1	0.041962745788105575	0.01617742288114674	0.02845031368729848	0.01100547288317344
2	0.10717746225992	0.08930616263474539	0.07053085455625973	0.05984825317707202
3	0.20024123115789	0.2396401470008922	0.1244662250449701	0.1559677956367871
4	0.35622568741554	0.5102849384064862	0.2021047007456418	0.3165723758668845
5	0.6604787100025195	1.0000000000000000	0.3261128629248666	0.5753698412085129
6	1.36804295333940783	1.959689429836578	0.5458501735606061	1.000000000000000
7	3.48685872889035930	4.172923495979481	0.9850850802286254	1.738012541463052
8	13.4381848942707415	11.9743554641257	2.016649317776546	3.158835312972759
9	160.340827693254954	61.81454285684810	5.116602053912441	6.411580005456822
10			19.69138119799427	16.70892543916556
11			234.8927672230579	90.86388296216937

the branch cut. Nevertheless, it works for cases away from the branch cut. In some cases, it may be desirable to place the branch cut in a different location, say along the ray $\arg(z) = \theta$. This is easily done by choosing the expansion point z_0 as $e^{-i\theta}$, as can be seen from Eq. (9). As long as there are no eigenvalues along the ray $\arg(z) = \theta$ for the matrix $\mathbf{M}$, one can apply the Padé approximation outlined above to calculate determinants which are negative or complex [15].

It is worth mentioning that the Padé approximation furnishes a much more accurate global approximation to the logarithm than that obtained from the "Green function" method [16].

The Green function approximation makes use of the fact that

$$\frac{1}{\pi} \lim_{\epsilon \to 0} \frac{1}{\lambda - \lambda_0 - \iota\epsilon} = \delta(\lambda - \lambda_0), \qquad (11)$$

whence it follows

$$\mathrm{Tr}\log \mathbf{M} = \int_{\lambda_{\min}}^{\lambda_{\max}} \log\lambda\, \rho(\lambda)\, d\lambda \qquad (12)$$

$$\approx \sum_i \log\lambda_i \frac{\Delta\lambda}{\pi} \,\mathrm{Im} \int_{\lambda_{\min}}^{\lambda_{\max}} \frac{\rho(\lambda)}{\lambda - \lambda_i - \iota\epsilon} d\lambda \qquad (13)$$

$$= \frac{1}{\pi} \sum_i \log\lambda_i \,\Delta\lambda\, \mathrm{Im}[\mathrm{Tr}(\mathbf{M} - \lambda_i - \iota\epsilon)^{-1}], \qquad (14)$$

where λ_i are evenly spaced on $[\lambda_{\min}, \lambda_{\max}]$, and ϵ is a small parameter.

This approximation may be rewritten as

$$\int_{\lambda_{\min}}^{\lambda_{\max}} \log\lambda\, \rho(\lambda)\, d\lambda \approx \int_{\lambda_{\min}}^{\lambda_{\max}} f_\epsilon(\lambda)\rho(\lambda)\, d\lambda, \qquad (15)$$

where

$$f_\epsilon(\lambda) = \frac{\Delta\lambda}{\pi} \sum_i \frac{\epsilon \log\lambda_i}{(\lambda - \lambda_i)^2 + \epsilon^2}. \qquad (16)$$

Figure 7 shows that the function $f_\epsilon(\lambda)$ with 11 terms and several ϵ furnishes a very poor approximation to the logarithm in the interval $1/60 < \lambda < 60$. By contrast, Fig. 2 shows
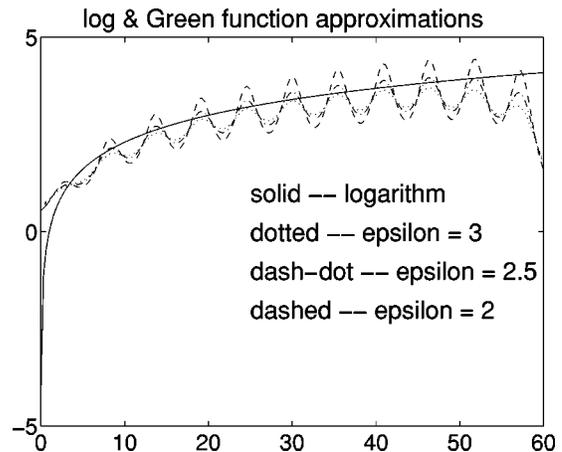
FIG. 7. Eleven-term Green function approximation to log with various ϵ, compared to the log function itself.

that an 11-term Padé expansion on the same interval approximates the logarithm to $\pm.0005$ at worst, and to much higher accuracy on most of the interval. Also, the Green function method is only applicable if the eigenvalues of the matrix are *real*, while the Padé approximation also holds for matrices with *complex* eigenvalues.

B. Complex Z_2 noise trace estimation

Exact computation of the trace inverse for $N \times N$ matrices is very time consuming for matrices of size $N \sim 10^6$. However, the complex Z_2 noise method has been shown to provide an efficient stochastic estimation of the trace [17,6,18]. In fact, it has been proved to be an optimal choice for the noise, producing a *minimum* variance [19,20].

The complex Z_2 noise estimator can be briefly described as follows [17,19]. We construct L noise vectors $\boldsymbol{\eta}^1, \boldsymbol{\eta}^2, \ldots, \boldsymbol{\eta}^L$ where each element $\eta_n^j, n=1,\ldots,N$ takes one of the four values $\{\pm 1, \pm \iota\}$ chosen independently with equal probability. It follows from the statistics of η_n^j that

$$E[\langle \eta_m^\star \eta_n \rangle] \equiv E\left[\frac{1}{L} \sum_{j=1}^L \eta_m^{\star j} \eta_n^j\right] = \delta_{mn}. \qquad (17)$$

The vectors can be used to construct an unbiased estimator for the trace inverse of a given matrix $\mathbf{A}$ as follows:

$$\begin{aligned}
E[\langle \boldsymbol{\eta}^\dagger \mathbf{A}^{-1} \boldsymbol{\eta} \rangle] &\equiv E\left[\frac{1}{L} \sum_{j=1}^L \sum_{m,n=1}^N \eta_m^{\star j} A_{m,n}^{-1} \eta_n^j\right] \\
&= \frac{1}{L} \sum_{j=1}^L \left(\sum_{n=1}^N A_{n,n}^{-1}\right) E[\eta_n^{\star j} \eta_n^j] \\
&\quad + \frac{1}{L} \sum_{j}^L \left(\sum_{m \neq n}^N A_{m,n}^{-1}\right) E[\eta_m^{\star j} \eta_n^j] \\
&= \sum_n^N A_{n,n}^{-1} + \left(\sum_{m \neq n}^N A_{m,n}^{-1}\right) E\left[\frac{1}{L} \sum_j^L \eta_m^{\star j} \eta_n^j\right] \\
&= \mathrm{Tr}\mathbf{A}^{-1}.
\end{aligned}$$

The variance of the estimator is shown to be [19]

$$\begin{aligned}
\sigma_A^2 &\equiv \mathrm{Var}[\langle \boldsymbol{\eta}^\dagger \mathbf{A}^{-1} \boldsymbol{\eta} \rangle] = E[|\langle \boldsymbol{\eta}^\dagger \mathbf{A}^{-1} \boldsymbol{\eta} \rangle - \mathrm{Tr}\mathbf{A}^{-1}|^2] \\
&= \frac{1}{L} \sum_{m \neq n}^N A_{m,n}^{-1}(A_{m,n}^{-1})^\star = \frac{1}{L} \sum_{m \neq n}^N |A_{m,n}^{-1}|^2.
\end{aligned}$$

The stochastic error of the complex Z_2 noise estimate results only from the off-diagonal entries of the inverse matrix (the same is true for Z_n noise for any n). However, other noises (such as Gaussian) have additional errors arising from diagonal entries. This is why the Z_2 noise has minimum variance. For example, it has been demonstrated on a $16^3 \times 24$ lattice with $\beta=6.0$ and $\kappa=0.148$ for the Wilson action that the Z_2 noise standard deviation is smaller than that of the Gaussian noise by a factor of 1.54 [17].

Applying the complex Z_2 estimator to the expression for the determinant ratio in Eq. (7), we find

$$\sum_k b_k\{\mathrm{Tr}(\mathbf{M}_1 + c_k\mathbf{I})^{-1} - \mathrm{Tr}(\mathbf{M}_2 + c_k\mathbf{I})^{-1}\}$$

$$\approx \frac{1}{L} \sum_k^K \sum_j^L b_k \boldsymbol{\eta}^{j\dagger}[(\mathbf{M}_1 + c_k\mathbf{I})^{-1} - (\mathbf{M}_2 + c_k\mathbf{I})^{-1}] \boldsymbol{\eta}^j$$

$$= \frac{1}{L} \sum_j^L \sum_{k=1}^K b_k \boldsymbol{\eta}^{j\dagger}(\boldsymbol{\xi}_1^{k,j} - \boldsymbol{\xi}_2^{k,j}), \qquad (18)$$

where $\boldsymbol{\xi}_i^{k,j} = (\mathbf{M}_i + c_k\mathbf{I})^{-1} \boldsymbol{\eta}^j$ are the solutions of

$$(\mathbf{M}_1 + c_k\mathbf{I})\boldsymbol{\xi}_1^{k,j} = \boldsymbol{\eta}^j, \qquad (19)$$

$$(\mathbf{M}_2 + c_k\mathbf{I})\boldsymbol{\xi}_2^{k,j} = \boldsymbol{\eta}^j, \quad k,j = 1,2,\ldots. \qquad (20)$$

Since $\mathbf{M}_i + c_k\mathbf{I}$ are shifted matrices with constant diagonal matrix elements, Eqs. (19) and (20) can be solved collectively for all values of c_k within one iterative process by several algorithms, including the quasi-minimum residual (QMR) [21], multiple-mass minimum residual (M^3R) [22], and generalized minimum residual (GMRES) [23] algorithms. We have adopted the M^3R algorithm, which has been shown to be about 2 times faster than the conjugate gradient algorithm, and the overhead for the multiple c_k is only 8% [24]. The only price to pay is memory: For each c_k, a single solution vector needs to be stored. Furthermore, since $c_k > 0$ (see Table I) and the eigenvalues of $\mathbf{M}$ have positive real parts, the conditioning of $(\mathbf{M} + c_k\mathbf{I})$ is improved and we should expect faster convergence for the column inversions in Eqs. (19) and (20).

In the HMC algorithm, if $\mathbf{M}_1$ and $\mathbf{M}_2$ denote quark matrices at the beginning and end of a molecular dynamics trajectory, we have $\mathrm{Tr}\log\mathbf{M}_1 - \mathrm{Tr}\log\mathbf{M}_2 = \sim\mathcal{O}(1)$. Hence, we need to reduce the error of the Z_2 noise estimate of the trace log difference to below $\sim\mathcal{O}(1)$. However, in practice we find that $\sim 319\,000$ noise vectors are required to reduce the stochastic error to 0.2. In the next section, we describe a method which significantly reduces the stochastic error.

III. IMPROVED PZ ESTIMATION WITH UNBIASED SUBTRACTION

In order to reduce the variance of the estimate, we introduce a suitably chosen set of traceless $N \times N$ matrices $\mathbf{Q}^{(p)}$, i.e. which satisfy $\Sigma_{n=1}^N \mathbf{Q}_{n,n}^{(p)} = 0$, $p=1,\ldots,P$. The expected value and variance for the modified trace estimator $\langle \boldsymbol{\eta}^\dagger(\mathbf{A}^{-1} - \Sigma_{p=1}^P \lambda_p \mathbf{Q}^{(p)}) \boldsymbol{\eta} \rangle$ are given by

$$E\left[\left\langle \boldsymbol{\eta}^\dagger \left(\mathbf{A}^{-1} - \sum_{p=1}^P \lambda_p \mathbf{Q}^{(p)}\right) \boldsymbol{\eta} \right\rangle\right] = \mathrm{Tr}\mathbf{A}^{-1}, \qquad (21)$$

$$\sigma_A^2(\boldsymbol{\lambda}) \equiv \mathrm{Var}\left[\left\langle \boldsymbol{\eta}^\dagger \left(\mathbf{A}^{-1} - \sum_{p=1}^P \lambda_p \mathbf{Q}^{(p)}\right) \boldsymbol{\eta} \right\rangle\right]$$

$$= \frac{1}{L} \sum_{m \neq n} \left|A_{m,n}^{-1} - \sum_{p=1}^P \lambda_p \mathbf{Q}_{m,n}^{(p)}\right|^2, \qquad (22)$$

for any values of the real parameters λ_p. In other words, introducing the matrices $\mathbf{Q}^{(p)}$ into the estimator produces no bias, but may reduce the error bars if the $\mathbf{Q}^{(p)}$ are chosen judiciously. Since the estimate $\langle \boldsymbol{\eta}^\dagger \mathbf{A}^{-1} \boldsymbol{\eta} \rangle$ actually denotes

TABLE II. Unimproved and improved PZ estimates for $\log[\det \mathbf{M}_1]$ with 100 complex Z_2 noise vectors. $\kappa = 0.150$.

$P[K,K](z)$	$K =$	5	7	9	11
$z_0 = 0.1$	Original	473(10)	774(10)	796(10)	798(10)
	Improved	487.25(62)	788.17(62)	810.83(62)	812.33(62)
$z_0 = 1.0$	Original	798(10)	798(10)	798(10)	799(10)
	Improved	812.60(62)	812.37(62)	812.36(62)	812.37(62)

an average of the independent, identically distributed random variables $\boldsymbol{\eta}^{j\dagger}\mathbf{A}^{-1}\boldsymbol{\eta}^{j}$, $j = 1,...,L$, we may minimize the variance $\sigma_A^2(\boldsymbol{\lambda})$ in Eq. (22) by choosing $\boldsymbol{\lambda}$ to minimize the variation of the numbers $\boldsymbol{\eta}^{j\dagger}(\mathbf{A}^{-1} - \Sigma_{p=1}^{P}\lambda_p \mathbf{Q}^{(p)})\boldsymbol{\eta}^{j}$, $j = 1,...,L$. This corresponds to a simple least-squares fit to the function $\boldsymbol{\eta}^{\dagger}\mathbf{A}^{-1}\boldsymbol{\eta}$ using the functions $\{1, \boldsymbol{\eta}^{\dagger}\mathbf{Q}^{(p)}\boldsymbol{\eta}\}$, $p = 1,...,P$, based on samples at points η_j, $j = 1,...,L$. Making the definition $\mathbf{Q}^{(0)} \equiv \mathbf{I}$, the usual least-squares equations then yield

$$\boldsymbol{\lambda} = \mathbf{C}^{-1}\boldsymbol{\alpha},$$

where

$$\boldsymbol{\lambda} \equiv (\lambda_0, \lambda_1, ..., \lambda_P)^T,$$

$$\mathbf{C}_{pq} \equiv \sum_{j=1}^{L} (\boldsymbol{\eta}^{j\dagger}\mathbf{Q}^{(p)}\boldsymbol{\eta}^{j})(\boldsymbol{\eta}^{j\dagger}\mathbf{Q}^{(q)}\boldsymbol{\eta}^{j}),$$

$$\alpha_q \equiv \sum_{j=1}^{L} (\boldsymbol{\eta}^{j\dagger}\mathbf{Q}^{(q)}\boldsymbol{\eta}^{j})(\boldsymbol{\eta}^{j\dagger}\mathbf{A}^{-1}\boldsymbol{\eta}^{j}),$$

and the trace estimate is given by $N\lambda_0$.

We now turn to the question of choosing suitable traceless matrices $\mathbf{Q}^{(p)}$ to use in the modified estimator. Equation (22) indicates that the matrices used should match the off-diagonal behavior of the matrix $\mathbf{A}$, so that they can cancel out the off-diagonal contributions to the variance. Since we

are using matrices of the form $\mathbf{A} = \mathbf{M} + c_k\mathbf{I}$, where $\mathbf{M} = \mathbf{I} - \kappa\mathbf{D}$ is the Wilson fermion matrix, one possible choice is suggested by the hopping parameter—κ expansion of the inverse matrix,

$$(\mathbf{M} + c_k\mathbf{I})^{-1} = \frac{1}{\mathbf{M} + c_k\mathbf{I}} = \frac{1}{(1+c_k)\left(\mathbf{I} - \frac{\kappa}{(1+c_k)}\mathbf{D}\right)}$$

$$= \frac{\mathbf{I}}{1+c_k} + \frac{\kappa}{(1+c_k)^2}\mathbf{D} + \frac{\kappa^2}{(1+c_k)^3}\mathbf{D}^2$$

$$+ \frac{\kappa^3}{(1+c_k)^4}\mathbf{D}^3 + \cdots . \qquad (23)$$

This suggests choosing the matrices $\mathbf{Q}^{(p)}$ from among those matrices in the hopping parameter expansion which are traceless:

$$\mathbf{Q}^{(1)} = \frac{\kappa}{(1+c_k)^2}\mathbf{D},$$

$$\mathbf{Q}^{(2)} = \frac{\kappa^2}{(1+c_k)^3}\mathbf{D}^2,$$

$$\mathbf{Q}^{(3)} = \frac{\kappa^3}{(1+c_k)^4}\mathbf{D}^3,$$

TABLE III. The variational parameters $\{\lambda\}_{opt}$ in Eq. (26) for different subtraction data set listed above and various Z_2 noise length L for $\mathbf{M}_1$.

Improved	Z_2 length	λ_1	λ_2	λ_3	λ_4	λ_5
1st	$L = 200$	0.960	—	—	—	—
	$L = 600$	0.968	—	—	—	—
2nd	$L = 200$	0.960	0.919	—	—	—
	$L = 600$	0.972	0.982	—	—	—
3rd	$L = 200$	0.968	0.942	0.908	—	—
	$L = 600$	0.972	0.969	0.919	—	—
4th	$L = 200$	0.973	0.921	0.903	1.23	—
	$L = 600$	0.976	0.924	0.967	1.21	—
5th	$L = 200$	0.990	0.926	0.908	1.21	1.27
	$L = 600$	0.992	0.924	0.910	1.19	1.26
11th	$L = 50$	0.998	0.913	0.968	1.20	1.06
	$L = 100$	0.992	0.890	0.953	1.17	1.48
	$L = 150$	0.995	0.886	0.939	1.17	1.18
	$L = 200$	0.999	0.923	0.951	1.16	1.09
	$L = 300$	0.997	0.924	0.934	1.19	1.06
	$L = 400$	0.998	0.925	0.959	1.20	1.07
	$L = 600$	1.001	0.923	0.964	1.16	1.00

TABLE IV. Central values for improved stochastic estimation of $\log[\det \mathbf{M}_1]$ and rth-order-improved jackknife errors δ_r are given for different numbers of Z_2 noise vectors. κ is 0.150 in this case.

Z_2 No.	50	100	200	400	600	800	1000	3000	10000
0th	802.98	797.98	810.97	816.78	815.89	813.10	816.53	813.15	812.81
δ_0	±14.0	±9.81	±7.95	±5.54	±4.47	±3.83	±3.41	±1.97	±1.08
1st	807.89	811.21	814.13	815.11	814.01	814.62	814.97	—	—
δ_1	±4.65	±3.28	±2.48	±1.84	±1.50	±1.29	±1.12	-	-
2nd	813.03	812.50	811.99	812.86	811.87	812.89	813.04	—	—
δ_2	±2.46	±1.65	±1.34	±1.01	±0.83	±0.72	±0.64	-	-
3rd	812.07	812.01	811.79	812.44	812.18	812.99	813.03	—	—
δ_3	±1.88	±1.31	±1.01	±0.74	±0.58	±0.51	±0.44	-	-
4th	812.28	812.52	812.57	812.86	812.85	813.25	813.40	—	—
δ_4	±1.20	±0.94	±0.68	±0.48	±0.39	±0.35	±0.30	-	-
5th	813.50	813.07	813.36	813.70	813.47	813.54	813.50	—	—
δ_5	±0.82	±0.62	±0.47	±0.34	±0.29	±0.25	±0.22	-	-
6th	813.54	813.23	813.22	813.28	813.20	813.37	813.26	—	—
δ_6	±0.67	±0.49	±0.35	±0.25	±0.21	±0.18	±0.16	-	-
7th	814.18	813.74	813.44	813.42	813.39	—	—	—	—
δ_7	±0.44	±0.36	±0.26	±0.19	±0.16	-	-	-	-
9th	813.77	813.62	813.49	813.40	813.43	—	—	—	—
δ_9	±0.40	±0.30	±0.22	±0.16	±0.14	-	-	-	-
11th	813.54	813.41	813.45	813.44	813.43	—	—	—	—
δ_{11}	±0.38	±0.27	±0.21	±0.15	±0.13	-	-	-	-

$$\mathbf{Q}^{(4)} = \frac{\kappa^4}{(1+c_k)^5}(\mathbf{D}^4 - \text{Tr}\mathbf{D}^4),$$

$$\mathbf{Q}^{(5)} = \frac{\kappa^5}{(1+c_k)^6}\mathbf{D}^5,$$

$$\mathbf{Q}^{(6)} = \frac{\kappa^6}{(1+c_k)^7}(\mathbf{D}^6 - \text{Tr}\mathbf{D}^6),$$

$$\mathbf{Q}^{(2r+1)} = \frac{\kappa^{2r+1}}{(1+c_k)^{2r+2}}\mathbf{D}^{2r+1}, \quad r = 3,4,5,\dots .$$

It may be verified that all of these matrices are traceless. In principle, one can include all the even powers, which entails the explicit calculation of all the allowed loops in $\text{Tr}D^{2r}$. In this paper we have only included $\mathbf{Q}^{(4)}$, $\mathbf{Q}^{(6)}$, and $\mathbf{Q}^{(2r+1)}$. Note that $\text{Tr}\mathbf{D}^4$ in $\mathbf{Q}^{(4)}$ can be evaluated from

TABLE V. The same as in Table IV for $\log[\det \mathbf{M}_2]$.

Z_2 No.	50	100	200	400	600	800	1000	3000	10000
0th	788.96	793.87	809.08	813.03	813.06	811.14	815.29	811.48	809.54
δ_0	±15.8	±10.7	±8.27	±5.89	±4.66	±3.94	±3.46	±1.99	±1.09
1st	808.94	814.00	811.94	811.85	811.73	811.77	812.22	—	—
δ_1	±5.00	±3.69	±2.69	±1.91	±1.53	±1.39	±1.25	-	-
2nd	810.75	811.11	810.29	810.21	810.15	810.43	811.05	—	—
δ_2	±2.67	±1.94	±1.40	±1.03	±0.84	±0.73	±0.66	-	-
3rd	806.65	808.13	809.28	809.58	810.06	810.56	810.52	—	—
δ_3	±1.79	±1.36	±1.01	±0.69	±0.56	±0.48	±0.43	-	-
4th	807.80	808.89	810.02	809.76	810.06	810.32	810.40	—	—
δ_4	±1.17	±0.97	±0.69	±0.49	±0.39	±0.33	±0.30	-	-
5th	809.92	809.80	810.55	810.68	810.82	810.85	810.79	—	—
δ_5	±0.89	±0.69	±0.52	±0.37	±0.29	±0.25	±0.22	-	-
7th	810.47	809.93	810.65	810.58	810.74	—	—	—	—
δ_7	±0.75	±0.62	±0.46	±0.32	±0.25	-	-	-	-
9th	809.04	809.90	810.70	810.71	810.80	—	—	—	—
δ_9	±0.66	±0.59	±0.43	±0.29	±0.23	-	-	-	-
11th	810.02	809.73	810.65	810.71	810.81	—	—	—	—
δ_{11}	±0.65	±0.56	±0.42	±0.29	±0.23	-	-	-	-
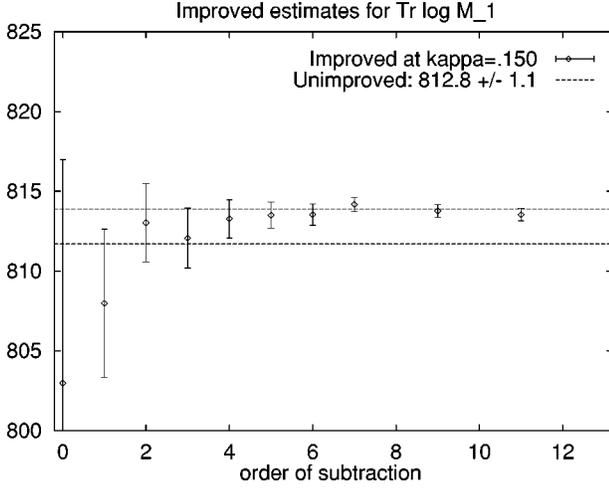
FIG. 8. The improved PZ estimate of Tr log $\mathbf{M}_1$ with 50 noises as a function of the order of subtraction and compared to that of unimproved estimate with 10 000 noises. The dashed lines are drawn with a distance of 1σ away from the central value of the unimproved estimate.

$$\mathrm{Tr}\mathbf{D}^4 = -32\sum_p \mathrm{Tr}\mathbf{U}_p, \tag{24}$$

where $\mathrm{Tr}\mathbf{U}_p$ is the plaquette and -32 comes from the trace of the product of $1 \pm \gamma_\mu$ in the the Wilson action. Similarly, $\mathrm{Tr}\mathbf{D}^6$ in $\mathbf{Q}^{(6)}$ can be evaluated from 3 classes of 6-link loops,

$$\mathrm{Tr}\mathbf{D}^6 = -128\sum_{L_1 \in R} U_{L_1} - 64\sum_{L_2 \in P} U_{L_2} - 64\sum_{L_3 \in C} U_{L_3}, \tag{25}$$
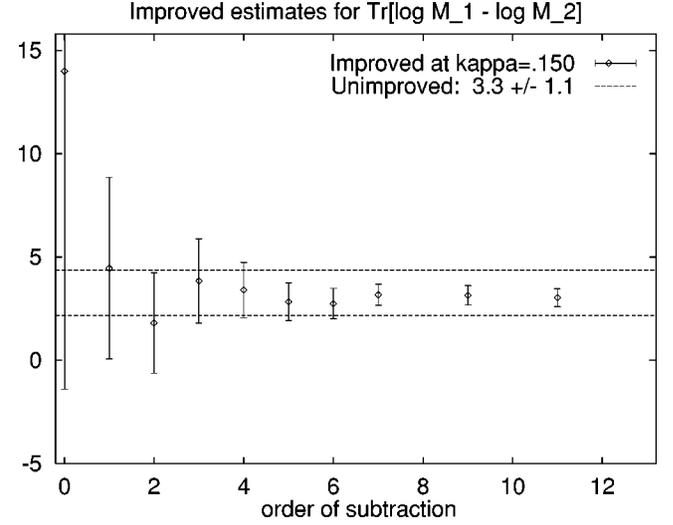
FIG. 9. Same as Fig. 8, for $\mathrm{Tr}[\log \mathbf{M}_1 - \log \mathbf{M}_2]$ with $\kappa = 0.150$.

where L_1 stands for the sum over rectangles, L_2 over parallelograms, and L_3 over chairs.

We then set

$$\mathbf{Q}(\boldsymbol{\lambda}) = \lambda_1 \mathbf{Q}^{(1)} + \lambda_2 \mathbf{Q}^{(2)} + \lambda_3 \mathbf{Q}^{(3)} + \lambda_4 \mathbf{Q}^{(4)} + \lambda_5 \mathbf{Q}^{(5)} + \lambda_6 \mathbf{Q}^{(6)}$$
$$+ \cdots + \lambda_{2r+1}\mathbf{Q}^{(2r+1)} + \cdots, \tag{26}$$

and perform the variation process to get an optimal choice of $\{\lambda_1, \lambda_2, \ldots, \lambda_{2r+1}, \ldots\}_{opt}$. The additional computational cost incurred by the modified estimator is P additional matrix vector multiplications per noise vector. Since P is small (~ 9), this overhead is essentially negligible compared to solving Eqs. (19) and (20).

TABLE VI. The same as in Table IV for $\log[\det \mathbf{M}_1 / \det \mathbf{M}_2]$.

L	50	100	200	400	600	800	1000	3000	10000
0th	14.0	4.12	1.90	3.75	2.84	1.96	1.24	1.67	3.28
δ_0	± 15.4	± 11.5	± 8.20	± 5.59	± 4.68	± 4.01	± 3.54	± 2.06	± 1.13
1st	4.46	2.39	2.30	3.23	2.24	2.85	2.75	3.16	—
δ_1	± 4.40	± 3.56	± 2.75	± 1.99	± 1.67	± 1.45	± 1.31	± 0.75	-
2nd	1.81	1.49	1.72	2.62	1.75	2.45	1.99	3.05	—
δ_2	± 2.43	± 1.98	± 1.49	± 1.11	± 0.95	± 0.82	± 0.73	± 0.42	-
3rd	3.85	2.72	2.45	2.78	2.16	2.43	2.48	3.04	—
δ_3	± 2.04	± 1.45	± 1.05	± 0.76	± 0.63	± 0.54	± 0.48	± 0.27	-
4th	3.41	2.77	2.51	3.04	2.81	2.92	2.99	—	—
δ_4	± 1.34	± 0.97	± 0.70	± 0.51	± 0.42	± 0.36	± 0.33	-	-
5th	2.84	2.84	2.75	2.95	2.62	2.68	2.70	—	—
δ_5	± 0.91	± 0.65	± 0.51	± 0.38	± 0.32	± 0.27	± 0.24	-	-
6th	2.75	2.80	2.65	2.65	2.49	2.54	2.51	—	—
δ_6	± 0.74	± 0.52	± 0.39	± 0.29	± 0.24	± 0.20	± 0.18	-	-
7th	3.18	3.27	2.77	2.90	2.77	—	—	—	—
δ_7	± 0.51	± 0.35	± 0.27	± 0.21	± 0.18	-	-	-	-
9th	3.15	3.39	2.78	2.81	2.76	—	—	—	—
δ_9	± 0.47	± 0.32	± 0.25	± 0.19	± 0.16	-	-	-	-
11th	3.04	3.33	2.76	2.83	2.72	—	—	—	—
δ_{11}	± 0.44	± 0.29	± 0.23	± 0.17	± 0.14	-	-	-	-

TABLE VII. Same as Table VI for the $\log[\det \mathbf{M}_1/\det \mathbf{M}_2]$ at $\kappa = .154$ instead of $\kappa = .150$.

Z_2 No.	50	100	200	400	600	800	1000	3000	10000
0th	12.6	2.66	2.32	4.86	3.84	2.68	1.92	3.35	4.31
δ_0	± 16.3	± 12.0	± 8.53	± 5.83	± 4.86	± 4.18	± 3.68	± 2.15	± 1.19
1st	-0.45	-1.60	3.56	4.67	3.27	4.11	4.04	—	—
δ_1	± 5.09	± 3.88	± 2.96	± 2.16	± 1.79	± 1.55	± 1.39	-	-
2nd	3.54	3.21	3.17	4.14	2.88	3.70	3.32	—	—
δ_2	± 2.81	± 2.27	± 1.66	± 1.26	± 1.08	± 0.93	± 0.69	-	-
3rd	6.27	5.07	3.90	4.32	3.58	3.84	3.94	—	—
δ_3	± 2.30	± 1.65	± 1.20	± 0.89	± 0.74	± 0.64	± 0.57	-	-
4th	5.49	5.22	4.28	4.73	4.46	4.49	4.49	—	—
δ_4	± 1.58	± 1.13	± 0.54	± 0.64	± 0.52	± 0.45	± 0.41	-	-
5th	4.55	4.72	4.30	4.35	4.01	4.10	4.08	—	—
δ_5	± 1.07	± 0.77	± 0.63	± 0.49	± 0.41	± 0.35	± 0.32	-	-
6th	4.51	4.72	4.12	4.03	3.83	3.91	3.88	—	—
δ_6	± 0.91	± 0.68	± 0.54	± 0.42	± 0.34	± 0.29	± 0.26	-	-
7th	5.13	5.52	4.35	4.43	4.24	4.16	4.02	—	—
δ_7	± 0.77	± 0.55	± 0.44	± 0.35	± 0.28	± 0.24	± 0.22	-	-
9th	4.98	5.60	4.33	4.27	4.21	4.16	4.08	—	—
δ_9	± 0.67	± 0.52	± 0.43	± 0.32	± 0.26	± 0.22	± 0.20	-	-
11th	4.80	5.60	4.32	4.31	4.19	4.21	4.13	—	—
δ_{11}	± 0.64	± 0.49	± 0.42	± 0.31	± 0.25	± 0.21	± 0.19	-	-

In actual practice, we generate L complex Z_2 noise vectors, and obtain basic Padé-Z_2 (PZ) estimates using the M^3R matrix inversion algorithm. The auxiliary data used in the improved PZ estimates may be computed via a few matrix-vector multiplications:

Unimproved estimates $\{O_1, O_2, \ldots, O_L\}$, with $O_j = \Sigma_k b_k \eta^{j\dagger} \xi_{k,j}$, $j = 1, 2, \ldots, L$.

First auxiliary data set $\{D_1^{(1)}, D_2^{(1)}, \ldots, D_L^{(1)}\}$, with $D_j^{(1)} = \Sigma_k [b_k \kappa/(1+c_k)^2] (\eta^{j\dagger} \mathbf{D} \eta^j)$.

Second auxiliary data set $\{D_1^{(2)}, D_2^{(2)}, \ldots, D_L^{(2)}\}$, with $D_j^{(2)} = \Sigma_k [b_k \kappa^2/(1+c_k)^3] (\eta^{j\dagger} \mathbf{D}^2 \eta^j)$.

Third auxiliary data set $\{D_1^{(3)}, D_2^{(3)}, \ldots, D_L^{(3)}\}$, with $D_j^{(3)} = \Sigma_k [b_k \kappa^3/(1+c_k)^4] (\eta^{j\dagger} \mathbf{D}^3 \eta^j)$.

Fourth auxiliary data set $\{D_1^{(4)}, D_2^{(4)}, \ldots, D_L^{(4)}\}$, with $D_j^{(4)} = \Sigma_k [b_k \kappa^4/(1+c_k)^5] (\eta^{j\dagger} \mathbf{D}^4 \eta^j - \mathrm{Tr}\mathbf{D}^4)$.

Fifth auxiliary data set $\{D_1^{(5)}, D_2^{(5)}, \ldots, D_L^{(5)}\}$, with $D_j^{(5)} = \Sigma_k [b_k \kappa^5/(1+c_k)^6] (\eta^{j\dagger} \mathbf{D}^5 \eta^j)$.

Sixth auxiliary data set $\{D_1^{(6)}, D_2^{(6)}, \ldots, D_L^{(6)}\}$, with $D_j^{(6)} = \Sigma_k [b_k \kappa^6/(1+c_k)^7] (\eta^{j\dagger} \mathbf{D}^6 \eta^j - \mathrm{Tr}\mathbf{D}^6)$.

Higher odd terms $\{D_1^{(2r+1)}, D_2^{(2r+1)}, \ldots, D_L^{(2r+1)}\}$, with $D_j^{(2r+1)} = \Sigma_k [b_k \kappa^{2r+1}/(1+c_k)^{2r+2}] (\eta^{j\dagger} \mathbf{D}^{2r+1} \eta^j)$.

Using these data, a least squares fit is performed to yield a set of $\{\lambda_0, \lambda_1, \lambda_2, \lambda_3, \lambda_4, \lambda_5, \lambda_6, \lambda_{(2r+1)}\}_{opt}$, which minimizes the variance Eq. (22) of the improved estimator over the $\{L\}$ noise vectors.

IV. COMPUTATIONS OF DETERMINANTS AND DETERMINANT RATIOS

Our numerical computations were carried out with the Wilson action on the $8^3 \times 12$ ($N = 73\,728$) lattice with $\beta = 5.6$. We use the HMC algorithm with pseudofermions to generate gauge configurations. With a cold start, we obtain

the fermion matrix $\mathbf{M}_1$ after the plaquette becomes stable. The trajectories are traced with $\tau = 0.01$ and 30 molecular dynamics steps using $\kappa = 0.150$. $\mathbf{M}_2$ is then obtained from $\mathbf{M}_1$ by an accepted trajectory run. Hence $\mathbf{M}_1$ and $\mathbf{M}_2$ differ by a continuum perturbation, and $\log[\det \mathbf{M}_1/\det \mathbf{M}_2] \sim \mathcal{O}(1)$.

We first calculate $\log \det \mathbf{M}_1$ with different orders of the Padé expansion around $z_0 = 0.1$ and $z_0 = 1.0$. We see from Table II that the 5th order Padé approximation does not give the same answer for two different expansion points, suggesting that its accuracy is not sufficient for the range of eigenvalues of $\mathbf{M}_1$, whereas the 11th order Padé approximation gives the same answer within errors. Thus, we shall choose $P[11,11](z)$ with $z_0 = 0.1$ to perform the calculations from this point on.

Table III shows the optimal choice of parameters λ_i, $i = 1, 5$, with different subtraction sets and various Z_2 noise lengths. The fact that $\lambda_i \sim 1.0$, $i = 1, 2, 3, 4, 5$ gives further evidence that the fluctuations due to the complex Z_2 noise are indeed introduced by the off-diagonal matrix elements.

In Tables IV and V, we give the results of improved estimations for $\mathrm{Tr} \log \mathbf{M}_1$ and $\mathrm{Tr} \log \mathbf{M}_2$, respectively. We see that the variational technique described above can reduce the data fluctuations by more than an order of magnitude. For example, the unimproved error $\delta_0 = 5.54$ in Table IV for 400 Z_2 noises is reduced to $\delta_{11} = 0.15$ for the subtraction which includes up to the $\mathbf{Q}^{11}$ matrix. This is 37 times smaller. Comparing the central values in the last row (i.e., the 11th order improved) with that of unimproved estimate with 10 000 Z_2 noises, we see that they are the same within errors. This verifies that the variational subtraction scheme that we employed does not introduce biased errors. The improved estimates of $\mathrm{Tr} \log \mathbf{M}_1$ from 50 Z_2 noises with errors δ_r from

Improved estimates for Tr[log M_1 - log M_2]
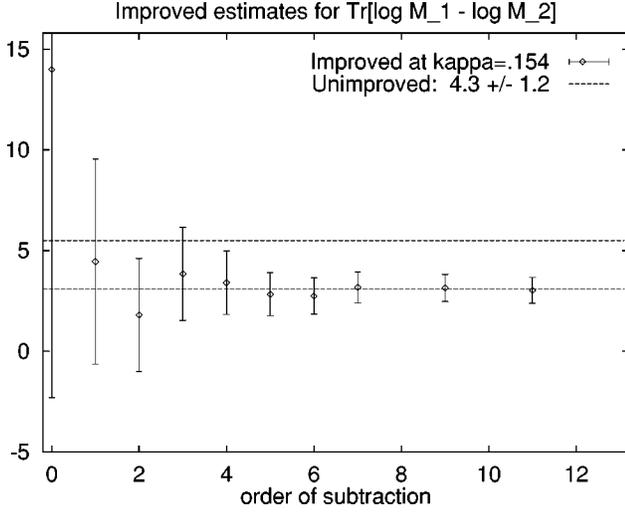
FIG. 10. Same as Fig. 9, for $\text{Tr}[\log \mathbf{M}_1 - \log \mathbf{M}_2]$ with $\kappa = 0.154$.

Table IV are plotted in comparison with the central value of the unimproved estimate from 10 000 noises in Fig. 8.

We note in passing that our unimproved results have the similar size errors as those obtained by the Chebyshev polynomial expansion of $\log \mathbf{M}^\dagger \mathbf{M}$ [1], and thus one can similarly improve its estimation with the variational subtraction scheme introduced here.

Results for $\text{Tr}[\log \mathbf{M}_1 - \log \mathbf{M}_2]$ are shown in Table VI. We see that again the errors are reduced by a factor ~ 34. δ_{11} for 50 Z_2 noise vectors is even smaller than the unimproved error δ_0 with $L = 10\,000$. To achieve the same level of accuracy for the unimproved estimation, it would require $\sim 65\,955$ noise vectors. This is 1319 times more than the 50 noise case which employs subtraction. Again, to show that the subtraction does not introduce biased errors, we plot in Fig. 9 the improved PZ estimates of $\text{Tr}[\log \mathbf{M}_1 - \log \mathbf{M}_2]$ with errors from 50 noise vectors as a function of the order of subtraction and verify that they agree with that of the unimproved estimate with 10 000 noises.

As for the quark mass dependence, one expects that the errors will go up as the quark mass becomes smaller. We have made an attempt to study this by considering the case of $\kappa = 0.154$ which corresponds to the strange quark mass and yields a π/ρ mass ratio of ~ 0.8. The results of $\text{Tr}[\log \mathbf{M}_1 - \log \mathbf{M}_2]$ are listed in Table VII. The PZ estimates and their errors in Table VII for $\kappa = 0.154$ are similarly plotted as a function of the order of subtraction in Fig. 10. We see that their errors are indeed larger than those in Table VI for the case of $\kappa = 0.150$ which gives a π/ρ mass ratio of ~ 0.9. For example, the error with 400 noises and 11th order subtraction for $\kappa = 0.154$ is 0.31 which is 82% larger than the corresponding error for $\kappa = 0.150$ at 0.17. Thus, this would require ~ 1325 noises (3.31 times of 400) for it to reach the same level of error as in the case of $\kappa = 0.150$. For still smaller quark mass, e.g. that corresponding to a π/ρ mass ratio of ~ 0.6, it may need tens of thousands of noises to reach an error at the same 17% level. Although this would account for an overhead of several trajectories at the accept-reject step if used in the hybrid Monte Carlo algorithm with determinant ratio [13], one hopes this

TABLE VIII. A breakdown of the energy change ΔH in 10 molecular dynamics trajectories in terms of the change in gauge action (ΔU_{plaq}), pseudofermion action (ΔU_{pseudo}), and kinetic energy ($\Delta \pi^2$). Also listed are the estimates of $\Delta(\text{Tr} \log \mathbf{M}) = \text{Tr} \log \mathbf{M}_1 - \text{Tr} \log \mathbf{M}_2$ using 600 Z_2 noises with subtraction. The κ is 0.150 in this case.

Group		ΔH(old-new)	$\Delta(\text{Tr} \log \mathbf{M})$
Pair 1	ΔU_{plaq}	-188.238	
M_1, M_2	ΔU_{pseudo}	15.636	$-0.21(.24)$
	$\Delta \pi^2$	172.514	
Pair 2	ΔU_{plaq}	437.556	
M_2, M_3	ΔU_{pseudo}	15.518	$-3.58(.26)$
	$\Delta \pi^2$	-453.023	
Pair 3	ΔU_{plaq}	-120.857	
M_3, M_4	ΔU_{pseudo}	-6.505	$0.56(.25)$
	$\Delta \pi^2$	127.331	
Pair 4	ΔU_{plaq}	-40.862	
M_4, M_5	ΔU_{pseudo}	-28.189	$2.03(.24)$
	$\Delta \pi^2$	69.085	
Pair 5	ΔU_{plaq}	-110.674	
M_5, M_6	ΔU_{pseudo}	-70.823	$-0.06(.24)$
	$\Delta \pi^2$	181.516	
Pair 6	ΔU_{plaq}	241.814	
M_6, M_7	ΔU_{pseudo}	67.498	$-3.69(.25)$
	$\Delta \pi^2$	-309.213	
Pair 7	ΔU_{plaq}	82.339	
M_7, M_8	ΔU_{pseudo}	-70.015	$-0.98(.24)$
	$\Delta \pi^2$	-12.315	
Pair 8	ΔU_{plaq}	-692.873	
M_8, M_9	ΔU_{pseudo}	-27.643	$6.51(.24)$
	$\Delta \pi^2$	720.243	
Pair 9	ΔU_{plaq}	260.435	
M_9, M_{10}	ΔU_{pseudo}	2.186	$-1.14(.25)$
	$\Delta \pi^2$	-262.522	
Pair 10	ΔU_{plaq}	-613.121	
M_{10}, M_{11}	ΔU_{pseudo}	110.997	$6.40(.24)$
	$\Delta \pi^2$	501.946	
Pair 11			
M_1, M_{11}			$5.85(.30)$

can be offset by a faster mapping of the topological charge space. This remains to be tested in future studies.

We have also generated a sequence of configurations through HMC updating with pseudofermions. In Table VIII we list the change of the gauge, the pseudofermion, and the kinetic energy parts of the action from 10 molecular dynamics trajectories. The total change in energy ΔH is $\sim O(1)$. Also listed are the change of $\text{Tr} \log \mathbf{M}$, i.e. $\Delta(\text{Tr} \log \mathbf{M}) = \text{Tr} \log \mathbf{M}_1 - \text{Tr} \log \mathbf{M}_2$. It is somewhat surprising to see that the absolute values of $\Delta(\text{Tr} \log \mathbf{M})$ are an order of magnitude smaller that those of ΔU_{pseudo} (the pseudofermion part of the action), and their signs can be different. This may be related to the observation that it takes very long to decorrelate the global topological charge in the HMC algorithm with pseudofermions [25]. This will be investigated further in the future.

V. APPLICATION TO GLOBAL DENSITY OF STATES FOR HERMITIAN HAMILTONIAN SYSTEMS

The density of states $\rho(z)$ for a Hamiltonian system with Hamiltonian matrix $\mathbf{H}$ is

$$\rho(z) = \frac{1}{N} \sum_{n=1}^{N} \delta(z - \lambda_n), \qquad (27)$$

where $\{\lambda_n\}$ are the eigenvalues of $\mathbf{H}$.

In Ref. [16], $\rho(z)$ for real z is calculated for Hermitian $\mathbf{H}$ as follows:

$$\rho(z) = \frac{1}{\pi} \lim_{\epsilon \to 0^+} \operatorname{Im} \operatorname{Tr}[\mathbf{H} - (z + \iota \epsilon)\mathbf{I}]^{-1}. \qquad (28)$$

Choosing a small ϵ in Eq. (28) yields a smoothed version of $\rho(z)$.

We have shown above that the trace in Eq. (28) may be estimated for several different values of z simultaneously using complex Z_2 noise and the M^3R algorithm. Thus, we may estimate the global density of states for a Hermitian matrix $\mathbf{H}$ at essentially the same computational cost (modulo additional memory) as estimating the local density of states at a single point.

VI. CONCLUSION AND SUMMARY OF ADVANTAGES OF THE PZ ALGORITHM

The PZ method takes advantage of proven, effective numerical approximation techniques. The advantages of the PZ method are summarized as follows:

The Padé approximation uses rational functions, which are known to be very efficient in the uniform approximation of analytic functions. In finding determinant ratios, the Padé approximation to the logarithm only needs to be accurate on the region in the complex plane where the spectra of $\mathbf{M}_1$ and $\mathbf{M}_2$ differ.

The complex Z_2 random vectors have been shown to be superior to the Gaussian [17,6,18] noise in computing traces of inverse matrices.

The PZ method also takes advantage of the recently developed M^3R algorithm to calculate all terms in the Padé expansion in Eq. (7) in essentially the same computational

time required to calculate a single term, albeit with additional memory (one length N vector for each additional term). Hence, a higher order Padé expansion requires more memory, but essentially the same computation time (apart from the matrix conditioning effects to be mentioned below).

The entire method can be applied to non-Hermitian matrices: So determinants of non-Hermitian matrices may also be found directly, without recourse to the Hermitian matrix $\mathbf{M}^\dagger\mathbf{M}$. Negative and complex determinants can also be calculated in principle.

The c_j's in the Padé expansion in Eq. (5) turn out to be real and positive, which improves the conditioning of the matrices $\mathbf{M} + c_j\mathbf{I}$ and hence expedites the column inversions in Eqs. (19), (20). However, this effect diminishes for higher order Padé approximations, because the minimum c_j decreases as the order increases.

The PZ method also holds promise of being useful in the case where different quark flavors are present, in which case it is necessary to compute multiple determinant ratios for matrices with different but constant diagonal terms. Using the M^3R algorithm, this takes essentially the same computation time as a single determinant ratio.

The unbiased variational subtraction scheme works quite well in reducing the stochastic error from the Z_2 noise. The principle is general enough to be applied to other cases with stochastic estimates.

In conclusion, we have demonstrated the efficiency of the Padé-Z_2 algorithm in estimating determinants and determinant ratios to high accuracy for lattice QCD. It is certainly applicable to other systems with large sparse matrices. For example, we have been able to reduce the error of the determinant ratio from 559% to 17% with the unbiased subtraction scheme and a relatively small (~ 400) number of the noise vectors (see Table VI). It is rather encouraging as far as the feasibility of using this algorithm to simulate dynamical fermions in full QCD is concerned. We shall pursue this in the future.

[1] J. Sexton and D. Weingarten, Phys. Rev. D **55**, 4025 (1997).

[2] F. Butler, H. Chen, J. Sexton, A. Vaccarino, and D. Weingarten, Phys. Rev. Lett. **70**, 2849 (1993); Nucl. Phys. **B430**, 179 (1994).

[3] For a review of heavy-light weak matrix elements, see J. Flynn, in *Lattice '96*, Proceedings of the International Symposium, St. Louis, Missouri, edited by C. Bernard *et al.* [Nucl. Phys. B (Proc. Suppl.) **53**, 168 (1997)].

[4] For a review of chiral perturbation theory and weak matrix elements, see S. Sharpe, in *Lattice '96* [3], p. 181.

[5] K. F. Liu, S. J. Dong, T. Draper, J. M. Wu, and W. Wilcox, Phys. Rev. D **49**, 4755 (1994); K. F. Liu, S. J. Dong, T. Draper, and W. Wilcox, Phys. Rev. Lett. **74**, 2172 (1995).

[6] S. J. Dong, J.-F. Lagaë, and K. F. Liu, Phys. Rev. Lett. **75**, 2096 (1995); S. J. Dong, J.-F. Lagaë, and K. F. Liu, Phys. Rev. D **54**, 5496 (1996).

[7] S. Sharpe, Phys. Rev. D **41**, 3233 (1990); **46**, 3146 (1992); J. Labrentz and S. Sharpe, *ibid.* **54**, 4595 (1996).

[8] C. Bernard and M. Golterman, Phys. Rev. D **46**, 853 (1992); **53**, 476 (1996).

[9] For a review of finite-temperature QCD on the lattice, see A. Ukawa, in *Lattice '96* [3], p. 106.

[10] D. Weingarten and D. Petcher, Phys. Lett. **99B**, 333 (1981); F. Fucito, E. Marinari, G. Parisi, and C. Rebbi, Nucl. Phys. **B180**, 369 (1981).

[11] M. Lüscher, Nucl. Phys. **B418**, 637 (1994).

[12] S. Duane, A. D. Kennedy, B. J. Pendleton, and D. Roweth, Phys. Lett. B **195**, 216 (1987).

[13] K. F. Liu, S. J. Dong, and C. Thron, in *Lattice '96* [3], p. 980.

[14] Z. Bai, M. Fahey, and G. Golub, J. Comput. Appl. Math. **74**, 71 (1996).

[15] C. Thron, K. F. Liu, and S. J. Dong, in *Lattice '96* [3], p. 977.

[16] S. Y. Wu, S. P. Bowen, and K. S. Dy, Solid State Mater. Sci. **10**, 43 (1980).

[17] Shao-Jing Dong and Keh-Fei Liu, Phys. Lett. B **328**, 130 (1994).

[18] SESAM Collaboration, N. Eicker *et al.*, Phys. Lett. B **389**, 720 (1996).

[19] S. Bernardson, P. McCarty, and C. Thron, Comput. Phys. Commun. **78**, 256 (1994).

[20] M. Hutchinson, Commun. Stat. Simul. **18**, 1059 (1989).

[21] A. Frommer, B. Nöckel, S. Güsken, Th. Lippert, and K. Schilling, Int. J. Mod. Phys. C **6**, 627 (1995).

[22] U. Glässner, S. Güsken, Th. Lippert, G. Ritzenhöfer, K. Schilling, and A. Frommer, hep-lat/9605008.

[23] A. Frommer and U. Glässner, SIAM (Soc. Ind. Appl. Math.) J. Sci. Stat. Comput. (to be published).

[24] He-Ping Ying, S. J. Dong, and K. F. Liu, in *Lattice '96* [3], p. 993.

[25] B. Allés, G. Boyd, M. D'Elia, A. Di Giacomo, and E. Vicari, Phys. Lett. B **389**, 107 (1996).